Materials Advances

ROYAL SOCIETY OF CHEMISTRY

PAPER

View Article Online
View Journal | View Issue

Cite this: *Mater. Adv.*, 2026, 7, 4149

A novel radiofrequency-induced phase-transition strategy for shape and stiffness switching in poly(glycerol dodecanoate) polymers

Kaixiang Jin, *[ab] Xiaomei Wu,[a] Sheng Hu,[b] Dajing Wu,[b] Ran Guo,[b] Zhichao Wang[b] and Yunxiao Liang[b]

Polyglycerol ester-based polymers (PGEs), characterized by unique properties such as thermo-responsive shape memory, mechanical properties matching those of soft tissues, and controllable biodegradability, are well-suited for minimally invasive smart implants targeting soft tissue applications. However, the phase-transition mechanism of the polymer relies on environmental temperature changes, introducing uncontrollable factors during implantation. In this study, nanoscale carbon black (CB) was used to modify the electrical conductivity of poly(glycerol dodecanoate) (PGD), one of the PGEs, enabling active radiofrequency (RF)-induced phase-transition behavior. Unlike the passive method triggered by body temperature, active phase transitions can enhance the operability of the implant during surgery. The relationship between polymer conductivity and electric field intensity on the phase-transition performances of PGD was investigated using a self-developed RF antenna. Through this approach, a PGD + 7wt%CB polymer was selected, achieving 30-second shape/stiffness switching effects at an RF intensity of 2200 V m^{-1} while maintaining mild thermal tissue damage (CEM43 = 14.33) during this period. This achievement provides a novel method for controlling the phase transition of PGEs, which can be further applied to the design and fabrication of the minimally invasive smart implants, such as intervertebral disc scaffolds, neural probes, and artificial muscles.

Received 29th December 2025,
Accepted 8th March 2026

DOI: 10.1039/d5ma01524c

rsc.li/materials-advances

Introduction

PGEs have been employed in the design and fabrication of minimally invasive smart implants due to their thermo-responsive shape memory, mechanical properties matching those of soft tissues, and controllable biodegradability.[1–3] This thermoset polymer is synthesized through a dehydration condensation reaction between fatty acids and glycerol. Depending on the carbon chain length of the fatty acids used, PGEs can be classified into various types, such as poly(glycerol sebacate) (PGS), PGD, and poly(glycerol tetradecanedioate) (PGT).[4–7] In our previous work, we designed and fabricated a tissue-engineered intervertebral disc scaffold using PGD, demonstrating good functional regeneration of nucleus pulposus in an intervertebral disc degeneration animal model.[2]

PGD is a typical semi-crystalline polymer like other shape memory polymers. The ratio between the crystalline and amorphous phases in the polymer can be modified through its crosslinking density, thereby influencing its phase-transition temperature.[8] This polymer exhibits markedly distinct mechanical properties across its phase-transition temperature.[9] Specifically, it exists in a rubbery state, similar to soft tissues, below the transition temperature and a more rigid glassy state above the transition temperature. The shape of the polymer can be programmed in a rubbery state and fixed in a glassy state. Upon reheating, the crystalline phase melts, allowing the polymer to revert to its original shape. The biodegradation properties of PGD can be controlled by leveraging surface erosion and enzymatic sensitivity of the polymer. As reported in our previous work, the degradation duration of the polymer can be adjusted from 8 to 16 weeks.[10]

However, the shape and stiffness switching effect of PGD relies on direct heat sources, such as body temperature, to induce the phase transition of the shape memory polymer. Body temperature-induced phase transfer always results in uncontrolled shape and stiffness switching for implantable devices during surgical procedures, which leads to implant misplacement or functional failure. Previous studies have modified PGEs with crosslinking properties induced by ultraviolet rays.[11–13] The required additional percutaneous access, such as ultraviolet exposure, further complicates the surgery

[a] College of Biomedical Engineering, Fudan University, Shanghai, China 200433. E-mail: kxjin@fudan.edu.cn
[b] Shanghai Institute of Medical Device Testing, Shanghai, 201318, China

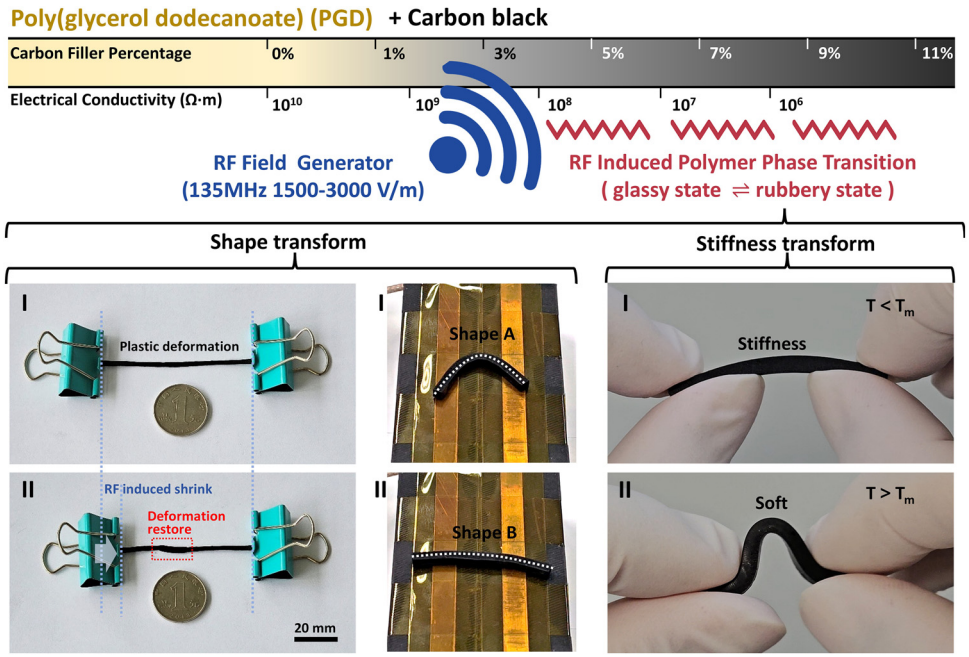

Fig. 1 RF-induced phase transition of PGD for shape and stiffness transformation.

and increases tissue damage. To solve the above limitation, indirect heat methods such as RF,[14] light,[15] and high-intensity focused ultrasound[16] were applied to achieve controllable phase transitions for shape memory polymers. RF heating is one of the indirect heat methods, and a self-heating phenomenon occurs in an implantable medical device made by conductive materials under the RF field during magnetic resonance imaging (MRI).[17] It can be utilized for implantable devices made by PGD or PGEs to achieve a wireless field-induced shape and stiffness switching effect.

This study aims to advance the medical utility of PGD by introducing shape and stiffness-switching properties triggered by the RF field, as shown in Fig. 1. To achieve this, nanoscale CB was selected and incorporated into PGD to obtain phase-transition capabilities under an RF field. The reason for choosing CB was because it not only efficiently enhanced the electrical conductivity of PGD but also possessed widely recognized biocompatibility; Establishing the correlations between synthesis properties of the polymer, RF parameters, and the phase-transition behavior of the modified polymer; Optimizing the phase-transition behavior of the PGD + CB polymer to ensure shape and stiffness property transform, and prevent tissue damage from heating during the period. The outcomes will further expand the clinical applicability of PGEs, improve the surgical handling of implants made by the PGD + CB polymer, and thus provide a feasible approach in minimally invasive smart implants, such as intervertebral disc scaffolds, stiffness-switchable neural electrode probes, and artificial muscles.

Methods

Polymer synthesis

The prepolymer of PGD was synthesized by glycerin and dodecanedioic acid (Sinopharm) with an equal molar ratio for 24 h as previously mentioned.[18] The prepolymers were then melted at 120 °C and stirred with 1 wt%, 3 wt%, 5 wt%, 7 wt%, 9 wt% or 11 wt% nano carbon black (BLACK PEARILS 2000) for another 48 h, respectively, as shown in Table 1 and Fig. S1. The viscous prepolymers were then poured into a Teflon dish and further esterified at 120 °C under a vacuum environment (−0.08 MPa), and then the polymer samples (disc shape with 60 mm

Table 1 Experimentally synthesized polymers in this study

	Composition proportion		Synthesis parameters		
Groups	PGD (wt%)	CB (wt%)	Curing temperature (°C)	Curing time (h)	Vacuum degree (MPa)
Pure PGD	100	0	120	0–192	−0.08
PGD + 1wt%CB	99	1	120	96	−0.08
PGD + 3wt%CB	97	3	120	96	−0.08
PGD + 5wt%CB	95	5	120	96	−0.08
PGD + 7wt%CB	93	7	120	96	−0.08
PGD + 9wt%CB	91	9	120	96	−0.08
PGD + 11wt%CB	89	11	120	96	−0.08

diameter, 3 mm thickness) were collected every 24 h until 196 h after the reaction. The collected polymer sample was stored at 4 °C to prevent degradation. A laser-cut machine (XTOOL P1) was used to cut the polymer disc into the required shape.

Thermodynamic properties

Thermodynamic properties of the polymers with 0 wt%–11 wt% carbon black were measured by differential scanning calorimetry (DSC) (DSC200, NETZSCH). The polymer samples were divided into seven groups based on their carbon filler percentages. There were 6 experimental groups with varying carbon black concentrations (1 wt%, 3 wt%, 5 wt%, 7 wt%, 9 wt%, and 11 wt%) and one control group without carbon black. The PGD polymer in each group was cured at 120 °C for 96 hours. A test sample weighing about 10 mg was cut from the polymer disc and sealed in an aluminum crucible. The crucible was put into a test chamber of DSC, heated to 80 °C and held for 1 minute, followed by a temperature scanning process. The temperature of the crucible was first cooled from 80 °C to −30 °C at the rate of 10 °C min^{-1}, then heated back to 80 °C. Heat flow during the temperature scanning process was recorded. The melting peak (T_m), crystallization peak (T_c) and fusion enthalpy (ΔH) were calculated using the Proteus software (NETZSCH). Isothermal crystallization tests were carried out to compare the crystallization of the PGD + CB polymer. The polymer was heated to 90 °C, and then cooled down to 45 °C (near T_m), 37 °C (body temperature), 25 °C (near room temperature), and 15 °C (near T_c), respectively, at the rate of 20 °C min^{-1}, and held at each temperature for 10 minutes. Heat flow during the period was recorded.

Mechanical properties

Young's modulus of the polymer was measured using a universal testing machine (ITBC-300SL, CARE) with a 10 N load cell and a water bath thermostat. The polymer was cut into a 40 × 3 × 3 mm strip-shaped sample. The polymer samples were divided into six experimental groups and one control group based on their carbon filler percentage. Each group was prepared with eight parallel samples; four samples were first warmed at a 50 °C-water bath to a melted polymer crystal and fully cooled back to 40 °C, then stretched to over 10% strain at a 40 °C-water bath at the speed of 1 mm min^{-1}. The remaining four samples were fully crystallized and warmed back to 25 °C, then stretched to breakage at room temperature at a speed of 1 mm min^{-1}. Mechanical tests were conducted at body temperature (37 °C). Polymer samples warmed from 25 °C to 37 °C and cooled from 45 °C to 37 °C were prepared separately. All the samples were kept at a 37 °C-water bath for over 10 min before the test. The samples were stretched to over 25% strain at a speed of 1 mm min^{-1}. The Young's modulus of each group was calculated based on the stress–strain curves and subjected to statistical analysis.

Cell viability

Polymer samples were sterilized at 121 °C for 30 minutes. The sterilized samples were immersed in Dulbecco's Modified Eagle Medium (DMEM) at a mass-to-volume ratio of 50 mg mL^{-1} and incubated at 37 °C for 24 hours to collect leach liquor. The leach liquor of each group was added to a 96-well plate. Pure PGD was the negative control group in this test. L929 cells were then seeded at a density of 1×10^4 cells per well into the plates. After 24 hours of co-culture, the cell viability was assessed using an MTT assay kit, and absorbance values for each group were measured using a microplate reader.

Electrical resistivity

An insulation resistance tester (HIOKI SM7110) was used to measure the electrical resistivity of the polymer samples. The PGD polymer with various carbon filler percentages from 0 wt% to 11 wt% was cut into 40 × 3 × 3 mm strip-shaped specimens and defined as seven experimental groups. Electrode slices were connected at both ends of the specimen. The resistance of the strip-shaped specimen was tested in the Ohm measurement mode at 500 V and an automatic current setting. Electrical resistivity ρ was calculated based on $\rho = R \times (A/L)$, where R, A, and L represent resistance, sectional area and length of the specimen, respectively. The electrical resistivity of each group was measured by four parallel samples, and mean values and standard deviations were calculated.

Optical observation

The polymer samples in each group were cut into 0.5 mm-thick slices using laser (P1, Xtool). An optical microscope (Zeta-20, Zeta) was used to observe the cross-section of PGD + CB polymers. Cross-sections of the polymer samples were observed under 5× and 20× magnifications and recorded using the image acquisition system of the microscope.

Electric field intensity test

As shown in Fig. 2A, a signal generator was used to produce a 135 MHz sinusoidal wave with a peak-to-peak voltage (V_{p-p}) of 0.1–0.2 V. A 200 W power amplifier was employed to amplify the sinusoidal signal. The amplified signal was then transmitted to the copper strips *via* a 50 Ω coaxial cable. An RF field over 1000 V m^{-1} was applied using an RF antenna composed by two parallel copper strips spaced only 12 mm apart, as shown in Fig. 2B. One copper strip was connected to the outer conductor of the coaxial cable, while the other was connected to the inner conductor. Each copper strip was embedded in insulating silicone. To reduce signal reflection during amplification and ensure antenna efficiency, impedance matching was applied to the RF antenna to achieve a return loss below −10 dB near 135 MHz.

An electromagnetic flowmeter (Safety Tech, EMS-01S) was used to monitor the intensity of the RF field. The electromagnetic flowmeter was fixed on a tripod, with the probe placed horizontally and freely movable in the vertical direction to adjust the distance between its probe and the RF antenna. Taking the midline between the two parallel copper strips as the mark point, the electric field intensity was measured at distances of 5, 10, 15, 20, 25, and 30 mm from the electrode. Additionally, output power could be regulated by adjusting

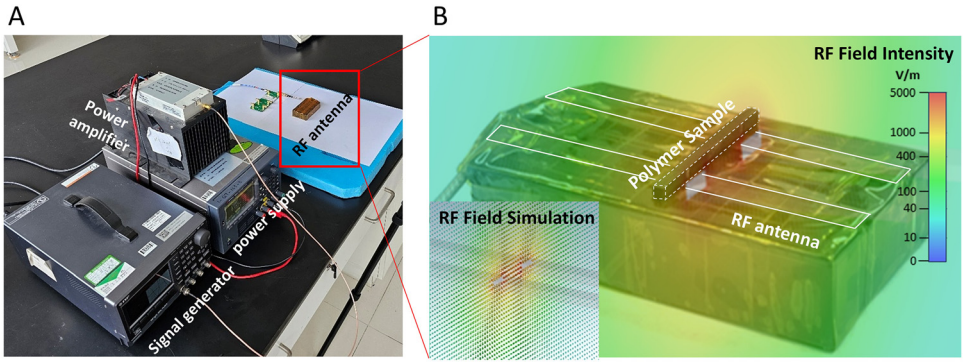

Fig. 2 Device with adjustable RF field intensity used in this study. (A) Basic composition of the experimental device. (B) RF antenna used to induce phase transition of the polymer sample and the simulation results of the RF field during experiments.

V_{p-p} of the signal from 0.05–0.20 V, and the electric field intensity under corresponding conditions was measured using the same setup. RF fields used in all experiments were either harmless to the human body or the surrounding environment, which were restricted following the Chinese national standard GB8702-2014.

The CST studio software (Dassault Systèmes) was used to simulate the electric field intensity of the parallel-plate antenna for comparison with the experimental results. The simulation model was established based on its real dimensions. The conductive medium was set as a perfect conductor, and the time-domain solver was used to analyze the electric field intensity around the antenna.

Heating rate of the polymer under the RF field

The surface temperature of the polymer sample was measured during the RF field heating process by an infrared camera (FLIR T620) and its data recording/analysis software (FLIR tools+). The infrared camera was fixed on a tripod at least 1 m apart from the polymer sample. The temperature field data of the polymer sample were recorded for at least 2 minutes starting from the RF field applied. The temperature of the middle part of the polymer sample was measured where was always the highest temperature area. Exporting the mean temperature of the measurement point during the RF field heating process, data for the polymer sample with various carbon filler percentages (0 wt%, 1 wt%, 3 wt%, 5 wt%, 7 wt%, 9 wt%, and 11 wt%) and electric field intensity (1500 V m^{-1}, 2200 V m^{-1}, and 3000 V m^{-1}) were analyzed separately.

Thermal damage evaluation

A tissue-mimicking gel was prepared with a conductivity of 0.47% ± 10% S m^{-1} based on ASTM F2182-2011a, closely matching human physiological characteristics. The gel was placed in a double-walled beaker, with a circulating water bath used to maintain the gel temperature at 37 °C. The RF antenna was positioned inside the gel, with the polymer sample spanning between plates. A radiofrequency signal was applied to the RF antenna to generate an electric field with an intensity of 2200 V m^{-1}. CEM43 is a general indicator used to assess the thermal damage of medical devices in the RF field. It was calculated as follows: $\mathrm{CEM43} = \sum_{i=1}^{n} t_i \times R^{(43-T_i)}$, where t represents the test duration, R is the empirical constant, and T is the temperature around the device. A fiber optic thermometer was used to measure the temperature between the polymer sample and the surrounding tissue-mimicking gel.

Statistical analysis

Experimental data for each group in this study were collected from 3–5 parallel samples, and shown as the mean value and standard deviation. Statistical differences among each group were determined using the Student's t-test. A P-value less than 0.05 was considered to indicate a statistically significant difference between the groups.

Results

Conductivity of the PGD + CB polymer

The resistivity of the PGD polymer is approximately 10^{10} Ω m, which exceeds the critical resistivity threshold of 10^{8} Ω m defined for insulators, thereby qualifying it as an insulating material. By mixing carbon black into its precursor, followed by stirring and thermal curing, composites with carbon filler percentages ranging from 1% to 11% were prepared. Fig. 3 presents the conductivity test results of these composites; as

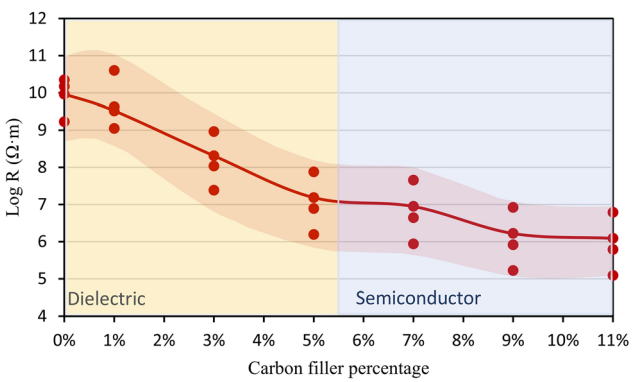

Fig. 3 Relationship between polymer resistivity and carbon filler loading.

the carbon filler percentage increased, the resistivity of the composites decreased from 10^{10} Ω m to approximately 10^{5} Ω m. Compared with pure PGD, the resistivity of the composites was significantly reduced. Although it did not reach the resistivity levels of common conductors (around 10^{-5} Ω m), a pronounced percolation effect was observed.

Uniformity of carbon black in the PGD + CB polymer

The uniformity of carbon black in polymers can be characterized by the electrical conductivity of polymers and the cross-sectional photographs. As shown in Fig. 4, the electrical conductivities of each group remained at the same order of magnitude, and no abnormal increase or decrease in conductance due to uneven mixing was observed.

As shown in Fig. S2, the black part represents carbon black in the polymer with lower light transmittance, while the white part indicates the PGD polymer with higher light transmittance. Each group of PGD + CB samples was relatively uniform, although it was still not perfect, which was related to the sedimentation of carbon black during the long-term curing process in the prepolymer. This phenomenon cannot be completely avoided because continuous stirring of the mixture is impossible for thermosetting polymers.

Thermodynamic properties of the PGD + CB polymer

Fig. 4 shows the DSC thermograms of the PGD + CB polymer with varying carbon filler percentages. As shown in Fig. 4A, the cooling process exhibited a T_c, while the heating process displayed a T_m, indicating a typical semi-crystalline polymer similar to pure PGD. The T_m, T_c, and ΔH among each group were almost unchanged, as shown in Fig. 4B, revealing that the phase-transition properties of PGD remain unchanged after carbon black filling (1–11%). As shown in Fig. 4C, with increasing curing time, both the crystallization/melting peak temperatures and the melting enthalpy of the composites gradually decreased. This aligned with our previous research,[18] suggesting a progressive reduction in the crystallinity of the polymer, which could be reflected in the decrease in enthalpy as the curing process progresses.

T_m plays a critical role in determining the phase-transition properties of the PGD + CB polymer. By varying the curing duration of the pre-polymer, T_m of the PGD + CB polymer was tuned from 36.2–52.3 °C. Meanwhile, the T_C of the PGD + CB polymer could be adjusted from 0.3 °C to 23.6 °C correspondingly. There was a temperature gap of over 20 °C between T_m and T_c. The temperature gap enabled the PGD + CB polymer in the rubbery state to retain its soft nature until the environmental temperature

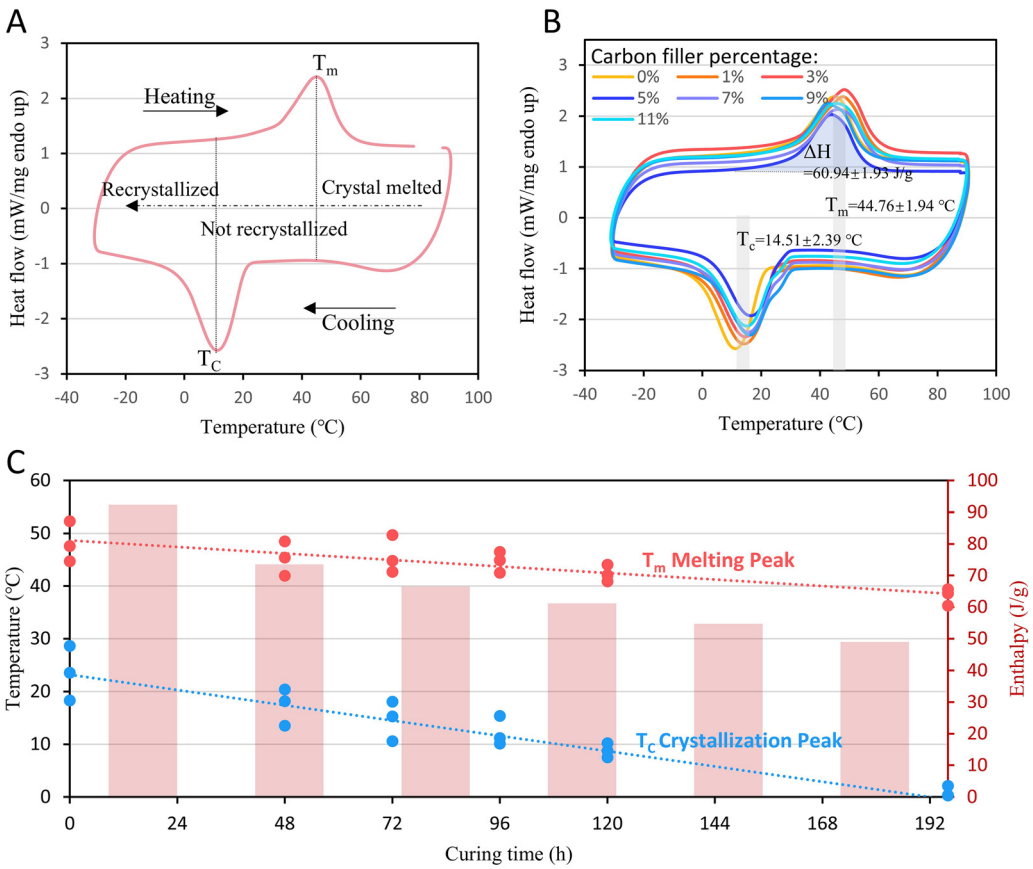

Fig. 4 Thermodynamic properties of PGD + CB polymers. (A) Crystallization and melting of PGD + CB polymers during a thermal cycling process; (B) thermodynamic properties of PGD + CB polymers remain unchanged among groups with various carbon filler percentages; and (C) crystallization/melting peak temperatures and the melting enthalpy of PGD + CB polymers gradually decreased with an increase in curing time.

decreased to T_c. Correspondingly, it also allowed the polymer in the glassy state to maintain its stiffness until the environmental temperature increased to T_m. Thus, the controlled phase transition of the PGD + CB polymer could be achieved *in vivo* when the T_m of the polymer was slightly above the body temperature (about 42 °C). In the particular condition, the polymer maintained its glassy state *in vivo* until the RF heating process was applied, inducing it to transform to a rubbery state.

Biocompatibility of the PGD + CB polymer

Leach liquor of the polymer sample was collected and used to culture L929 cells. As shown in Fig. 5, cell viability of the PGD polymer filled with 1 wt%–11 wt%CB was 81% ± 3.1%, 87% ± 3.7%, 81% ± 5.0%, 86% ± 2.6%, 86% ± 2.7%, and 86% ± 4.0%, which had no significant differences ($p > 0.05$) between each other or the pure PGD group (78% ± 4.5%). Pure PGD was proven to have no obvious cytotoxicity by *in-vitro* or *in-vivo* experiments in our previous research, which was used as a negative control group in this study.

Mechanical properties of the PGD + CB polymer

Mechanical properties of pure PGD and PGD + CB groups were measured at the glassy and rubbery state respectively. Typical stress–strain curves of the polymer in glassy and rubbery state were shown in Fig. S3A and B. In the glassy state, both of the pure PGD and PGD + CB polymer characterized plastic deformation behavior with over 100 MPa Young's modulus and over 120% strain before break. In the rubbery state, the polymer showed a linear elasticity with 300–1300 kPa Young's modulus, which was similar to soft tissue. With the increase of CB filled in PGD polymer, Young's modulus of the polymer gradually increased both in the glassy and rubbery state. The polymer also showed more brittleness at the same time.

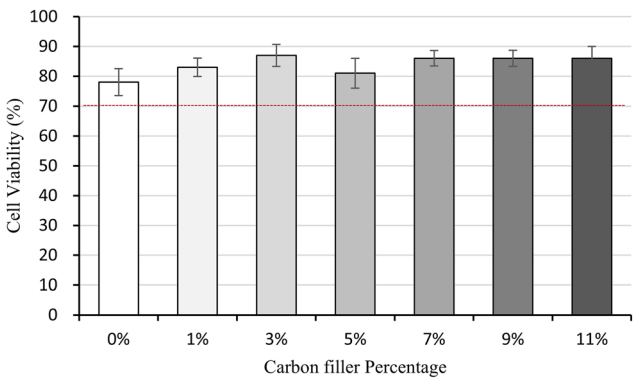

Fig. 5 Cell viability of PGD and PGD + CB polymers in the cytotoxicity test.

As shown in Table 2, Young's modulus and fracture strain of PGD + 1%CB were 125.27 ± 5.67 MPa and 280.32% ± 20.77% at the glassy state, which were similar to those of the pure PGD. Young's modulus of PGD + 11%CB was increased to 213.14 ± 21.03 MPa at the glassy state. Its fracture strain was significantly decreased to 77.65% ± 21.57%.

The Young's modulus of pure PGD was 290.33 ± 23.41 kPa at the rubbery state, with values comparable to those of PGD + 1%CB, PGD + 3%CB, PGD + 5%CB, and PGD + 7%CB polymers. While the Young's modulus of PGD + 9%CB and PGD + 11%CB was 920.92 ± 56.49 kPa and 1264.84 ± 115.03 kPa, respectively, in the rubbery state, demonstrating a significant increase when the CB content in the PGD polymer exceeded 9 wt%. This phenomenon might be related to the CB filler structure dominantly influencing the polymer network.

Adjusting the RF field intensity applied to the PGD + CB polymer

As shown in Fig. 6A, return loss characteristics of the RF antenna were evaluated across different frequencies before and after impedance matching. The impedance-matched antenna exhibited significantly improved efficiency, with a return loss of −20 dB at 135 MHz, indicating that most of the signal input power was effectively transmitted through the antenna rather than being reflected back to the amplifier. It represented a large improvement compared to the unmatched antenna, which had a return loss of only −0.2 dB.

The output power of the RF field was achieved by modulating the amplitude of the 135 MHz sinusoidal input signal, as shown in Fig. 6B. Peak-to-peak input voltages (V_{p-p}) of 0.1 V, 0.15 V, and 0.2 V generated corresponding output powers of approximately 1 W, 2 W, and 4 W, respectively. Meanwhile, the RF antenna produced an alternating RF field with maximum field intensity occurring along the central axis between the parallel plates, exhibiting a gradual attenuation with increasing distance from the centerline. RF field intensities at various output power and distance values were measured by experiments and simulation, respectively, as shown in Fig. 6C and D. Both the experimental and simulation results exhibited a similar trend. In detail, RF field intensities at 5 mm distance from the RF antenna surface were 1500 V m^{-1}, 2200 V m^{-1}, and 3000 V m^{-1} at 1 W, 2 W, and 4 W output power.

Table 2 Mechanical properties of PGD and PGD + CB polymers in glassy and rubbery states

Experimental groups		PGD	PGD + 1%CB	PGD + 3%CB	PGD + 5%CB	PGD + 7%CB	PGD + 9%CB	PGD + 11%CB
Glassy state at 25 °C	Young's modulus (MPa)	125.11 ± 6.61	125.27 ± 5.67	129.39 ± 10.32	139.95 ± 7.87	159.89 ± 10.74	183.11 ± 26.62	213.14 ± 21.03
	Fracture strain (%)	290.97 ± 14.93	280.32 ± 20.77	246.13 ± 35.42	197.24 ± 34.50	152.39 ± 27.71	122.26 ± 19.60	77.65 ± 21.57
Rubbery state at 40 °C	Young's modulus (kPa)	290.33 ± 23.41	307.66 ± 19.98	312.48 ± 20.13	404.50 ± 15.53	465.50 ± 30.26	920.92 ± 56.49	1264.84 ± 115.03

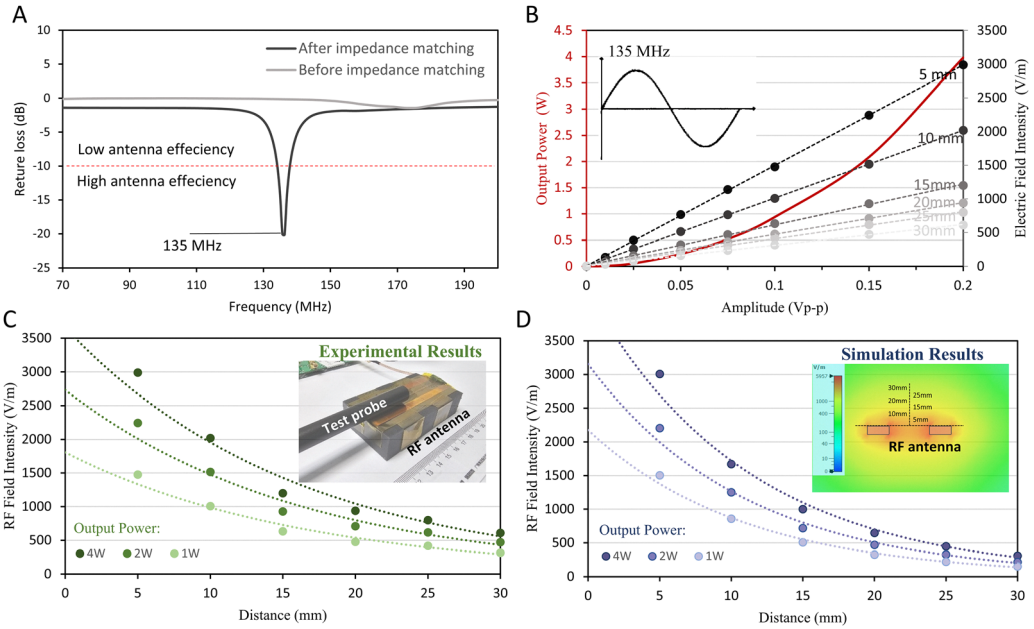

Fig. 6 Controlling the RF field intensity through physical parameters. (A) Adjusting RF efficiency by impedance matching of the parallel plate antenna. (B) Relationship among amplitude, distance, output power, and RF field intensity. RF field intensities at various output power and distance values measured by (C) experiments and (D) simulation.

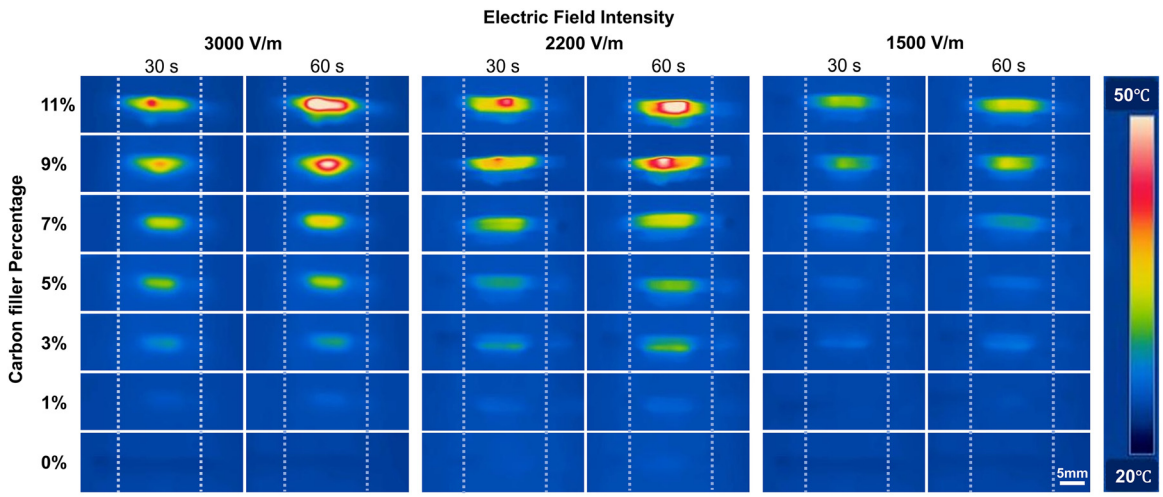

Fig. 7 Temperature changes of the polymer samples under the RF field with various intensities. Blue dotted lines represent the parallel plate antenna. The heating area is a rod-shaped sample that spans 5 mm above the parallel plates.

RF-induced heating effect of the PGD + CB polymer

RF-induced heating effect of the PGD polymer with varying carbon filler percentages was monitored through infrared thermography, as shown in Fig. 7. The pure PGD group exhibited a negligible temperature rise (<1 °C) under 3000 V m^{-1}, 2200 V m^{-1}, and 1500 V m^{-1} RF field intensities, whereas the PGD + CB polymer demonstrated progressively enhanced heating effect with both increasing carbon filler percentages and RF field intensities. In the 3000 V m^{-1} field intensity, the PGD + 11%CB group achieved rapid heating from 25 °C to 37 °C within 30 seconds, corresponding to a glassy state-to-rubbery state transition with the reduction in Young's modulus by three orders. 9%, 7%, 5%, 3%, and 1% group achieved heating from 25 °C to 35 °C, 33 °C, 32 °C, 30 °C, and 26 °C within 30 seconds. In the 2200 V m^{-1} field intensity, 11%, 9%, 7%, 5%, 3%, and 1% group achieved heating from 25 °C to 35 °C, 34 °C, 31 °C, 29 °C, 27 °C, and 26 °C within 60 seconds. In the 1500 V m^{-1} field intensity, 11%, 9%, 7%, 5%, 3%, and 1% group achieved heating from 25 °C to 32 °C, 30 °C, 28 °C, 26 °C, 25 °C, and 25 °C within 30 seconds.

Optimizing polymer and RF parameters for implant applications

The heating rate for each group is presented in Fig. 8A. It showed a positive correlation with carbon filler percentage

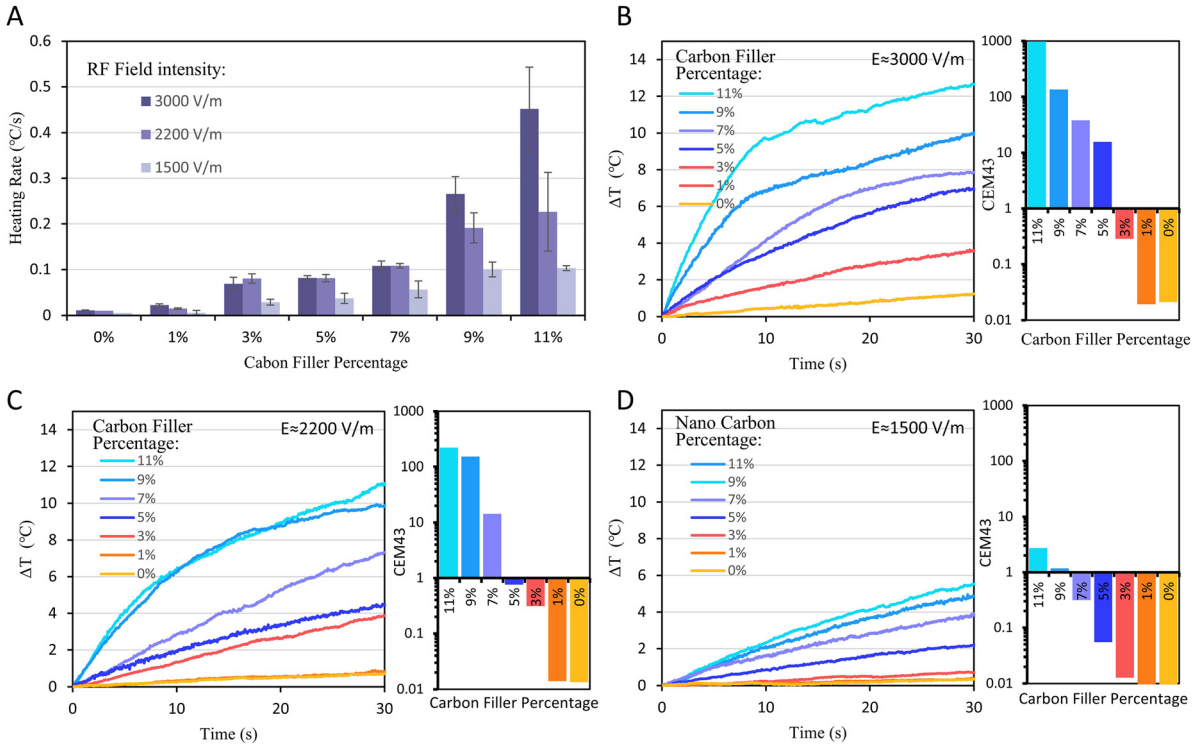

Fig. 8 Heating effects of the polymer samples induced by the RF field. (A) Heating rate of the polymer sample with different carbon filler percentages at RF fields with different intensities. RF field-induced heating effects of the polymer samples at (B) 3000 V m^{-1}, (C) 2200 V m^{-1}, and (D) 1500 V m^{-1} intensity.

and the RF field intensity. Thermal damage during the RF-induced heating was quantified by CEM43, as shown in Fig. 8B, C, and D. For the group PGD + 11%CB, the heating rates at high (3000 V m^{-1}), medium (2200 V m^{-1}), and low (1500 V m^{-1}) field intensity were 0.452, 0.227, and 0.103 °C s^{-1}, respectively, demonstrating the fastest heating efficiency and the fastest thermal damage at the same time; For the PGD + 7%CB group, the heating rates at high, medium, and low field intensities were 0.108, 0.107, 0.057 °C s^{-1}, respectively, demonstrating medium heating efficiency. CEM43 of the group remained at 0.32 to 38.29 in 30 s; For the PGD + 1%CB group, heating rates at high, medium, and low field intensities were 0.022, 0.015, 0.006 °C s^{-1}, respectively, demonstrating near imperceptible heating efficiency. CEM43 of the group remained at 0.01 to 0.02 in 30 s.

To balance heating efficiency and tissue thermal damage, a combination of the PGD + 7%CB polymer and 2200 V m^{-1} field intensity was selected as the optimal condition for conducting RF-induced phase transitions for implant devices. The combination exhibited moderate heating efficiency and conservative CEM43 (14.33), which was suitable for fabricating most of the implant devices. Supplementary Videos 1, 2, and 3 demonstrate the shape change, deformation restoration, and stiffness transition of PGD + 7%CB polymer induced under 2200 V m^{-1} field intensity.

Isothermal crystallization of the PGD + 7%CB polymer was measured at 45 °C (near T_m), 37 °C (body temperature), 25 °C (near room temperature), and 15 °C (near T_c), respectively, as shown in Fig. S4A. A distinct recrystallization peak occurred at 25 °C and 15 °C, while the polymers at 45 °C and 37 °C showed no obvious recrystallization during the period. This indicates that the PGD + 7%CB polymer would not revert to the glassy state after the RF-induced phase transition at body temperature. Mechanical tests were conducted to directly verify the above conclusion. As shown in Fig. S4B, the blue line represented the stress–strain curve of the PGD + CB polymer after RF heating and returning to body temperature. It exhibited typical linear elastic characteristics, indicating that the current polymer was in a typical rubbery state. On the contrary, the red line represented the stress–strain curve of the glassy polymer when heated to body temperature. It showed a significant deviation from the stress–strain curve of the polymer under the conditions described in this study. Thus, the optimized PGD + 7%CB polymer, which was subjected to an RF-induced phase transition, can remain in the rubber state at body temperature, meeting the application requirements for soft tissues.

Discussion

PGEs possess shape memory, biodegradability, and mechanical properties compatible with soft tissues. These characteristics distinguish PGEs from natural hydrogels with insufficient supporting capacity[19] and biodegradable polyesters with a rigid nature,[20] making them more suitable for minimally invasive smart implants applied to soft tissues. To improve

the operational performance of PGEs during implantation, this study introduced conductive modification of the PGD polymer, enabling controllable heating effect and phase transition under RF field exposure. An RF frequency at 135 MHz was selected as the working frequency of the modified PGD polymer, owing to its better tissue penetration depth due to a large wavelength and less tissue heating damage owing to low dielectric loss tangents, compared with microwave frequencies.[21–23]

PGD is a good insulator with an electrical resistivity of over 10^{10} Ω m. To exhibit RF-induced heating properties, the polymer should reduce its resistivity and be modified from an insulator to a dielectric or conductor.[24] Carbon black with nano particle scales is biocompatible, which is generally used for incorporation in polymers and could decrease resistivity by 3–5 orders, thereby obtaining an RF-induced heating effect.

In this study, the electrical conductivity of PGD was modified by uniformly incorporating nano-CB into the prepolymer of PGD, followed by curing the mixture at 120 °C under vacuum conditions for 96 h. PGD polymers filled with 1 wt%, 3 wt%, 5 wt%, 7 wt%, 9 wt%, and 11 wt%CB were fabricated to explore the correlation between the CB concentration and RF-induced heating effect. Physical properties of the fabricated PGD and PGD + CB polymer are shown in Table 3. A higher CB concentration in PGD over 11 wt% would lead to adverse formability during the polymer curing process. Thus, PGD with a CB concentration over 11 wt% was not selected as the experimental group. A notable improvement in electrical conductivity was observed in each PGD + CB group, resistivity decreasing from 10^{10} Ω m (PGD without CB) to 10^{6} Ω m (PGD + 11wt%CB). This indicated a transition in the polymer's electrical properties from an insulating state to a dielectric state that approximates conductive behavior.[24] Biodegradation duration of the PGD polymer was cited from our previously published work.[10] Both the *in-vitro* and *in-vivo* tests showed a linear degradation rate and about 9 weeks of degradation duration for the PGD polymer used in this study.

Incorporating CB did not significantly compromise the biocompatibility of biopolymers, as indicated in previous research.[25,26] Cytotoxicity tests revealed no statistically significant difference between PGD groups with 1–11 wt%CB and the pure PGD, as shown in Fig. 5.

Besides, the phase-transition property of the pure PGD and PGD + CB groups showed no significant difference. The transition temperature of the PGD polymer in this study has been tuned to near 42 °C, slightly above body temperature, by adjusting its synthesis temperature and curing time, as indicated in our previous research. Thus, the polymer was capable of transforming its phase from glassy state to rubbery state through a controllable RF field-induced heating effect. It could maintain the rubbery state in the body after RF ceased because the recrystallization temperature of the PGD polymer in this study was near 15 °C and lower than body temperature or its phase-transition temperature, as shown in Fig. S4.

To achieve controllable phase transitions of PGD + CB under RF fields, it is necessary to find the relationship between the RF field intensity and the heating rate of the polymer. A tunable RF field was generated by a pair of parallel plates. An RF field with a 135 MHz sine frequency and 1500–3300 V m^{-1} field strength could be output at 5 mm distance from the parallel plates by adjusting the input power (Fig. 6B). The heating rate of the PGD and PGD + CB groups was measured under field intensities of 1500 V m^{-1}, 2200 V m^{-1} and 3000 V m^{-1}, respectively. The results showed that the heating rate was positively correlated with the applied RF field intensity and the electrical conductivity of the polymer was as previously mentioned.[27]

To balance phase-transition efficiency and tissue damage caused by excessive heating rates, the polymer was set to achieve a temperature increase of 6–8 °C within 30 seconds under RF field exposure. This criterion enabled the identification of suitable PGD + CB groups and the corresponding RF field intensity in Fig. 8. Previous studies have been adopted to fabricate self-heating adhesives.[28] Distinct from adhesives, biological tissues exhibit a pronounced susceptibility to elevations in temperature resulting from polymers implanted therein or medical devices derived therefrom. Unusual heating may lead to irreversible tissue damage.[29] The PGD + 7wt%CB group with 2200 V m^{-1} field strength was selected based on the above conditions. A polymer sample of the PGD + 7wt%CB group was placed in a tissue-mimicking gel, a 2200 V m^{-1} RF field was applied for 30 seconds, and the CEM43 of the gel was measured during this process. The obtained CEM43 was 14.33, which was below the most stringent thermal damage threshold specified in ISO 14708-3, indicating its suitability for implantable devices.[30] Supplementary Videos 1 and 2 illustrate the shape and mechanical switching property caused by the phase transition before and after RF exposure. Based on the above-mentioned phase-transition characteristics, the PGD + CB polymer could be applied in fields such as stiffness-tunable

Table 3 Physical properties of PGD and PGD + CB polymers used in this study

	Thermodynamic property			Mechanical property		Electrical property	Biodegradation duration
	T_m	T_c (°C)	ΔH (J g^{-1})	E_{25} (MPa)	E_{40} (kPa)	Log ρ (Ω m)	
Pure PGD	44.5	11.2	61.8	125.1	290.3	10.2	~9 weeks[18]
PGD + 1wt%CB	47.9	14.2	63.9	125.3	307.7	9.6	—
PGD + 3wt%CB	43.9	16.2	60.8	129.4	312.5	7.4	—
PGD + 5wt%CB	46.2	15.8	57.7	139.9	404.5	6.9	—
PGD + 7wt%CB	42.6	16.7	59.7	159.9	465.5	6.6	—
PGD + 9wt%CB	42.6	16.0	61.2	183.1	620.9	5.9	—
PGD + 11wt%CB	44.9	11.2	62.1	213.1	1264.8	5.7	—

neural probes, minimally invasive implants, and artificial muscles. Furthermore, the polymer modification and performance modulation strategies presented in this study can be extended to other PGEs, thereby improving the surgical operability of polymer-based implantable devices.

This study still has some issues that require further *in vitro* and *in vivo* research for future applications, including biocompatibility of the released carbon particles during the polymer degradation, uniform distribution of carbon particles in the polymer, thermal damage evaluation during RF-induced phase transition of the polymer, and inflammatory responses of the polymer in the implanted tissue.

Author contributions

Research design: Kaixiang Jin and Xiaomei Wu. Material synthesis: Kaixiang Jin and Sheng Hu. Experimental tests and data analysis: Kaixiang Jin, Dajing Wu, Ran Guo, and Zhichao Wang. Cellular experiments and data analysis: Yunxiao Liang. Manuscript writing and editing: Kaixiang Jin, Xiaomei Wu, and Ran Guo.

Conflicts of interest

There are no conflicts to declare.

Data availability

The experimental data and simulation results that corroborate the findings of this study can be found in the figures and tables of the manuscript.

Supplementary information (SI): synthetic processes of PGD + CB polymer; cross section of the PGD + CB polymers; general mechanical properties of PGD + CB polymers; the properties of the PGD + CB polymer under different crystalline states. See DOI: https://doi.org/10.1039/d5ma01524c.

Acknowledgements

This study was supported by the China Postdoctoral Science Foundation (2024M752077), the Science and Technology Commission of Shanghai Municipality Strategic Frontier Special Project (24DP3201000), the State Key Laboratory of Brain-Machine Intelligence Open Research Project (BMI2400005) and the Shanghai Administration for Market Regulation Research Program (2025KJ78).

References

1 A. Mahjoubnia, D. Cai, Y. Wu, S. D. King, P. Torkian, A. C. Chen, R. Talaie, S.-Y. Chen and J. Lin, *Acta Biomater.*, 2024, **177**, 165–177.
2 L. Wang, K. Jin, N. Li, P. Xu, H. Yuan, H. Ramaraju, S. J. Hollister and Y. Fan, *Nat. Commun.*, 2023, **14**, 3865.
3 Z. Wu, K. Jin, L. Wang and Y. Fan, *Macromol. Biosci.*, 2021, **21**, e2100022.
4 S. Damle and C. Madankar, *Tenside, Surfactants, Deterg.*, 2023, **60**, 611–621.
5 M. Zhang and G. Zhang, *Polymers*, 2025, **17**, 879.
6 Y. Wang, G. A. Ameer, B. J. Sheppard and R. Langer, *Nat. Biotechnol.*, 2002, **20**, 602–606.
7 F. Migneco, Y. C. Huang, R. K. Birla and S. J. Hollister, *Biomaterials*, 2009, **30**, 6479–6484.
8 C. Zhang, H. Deng, S. M. Kenderes, J. W. Su, A. G. Whittington and J. Lin, *ACS Appl. Mater. Interfaces*, 2019, **11**, 5393–5400.
9 L. D. Solorio, M. L. Bocks and S. J. Hollister, *J. Biomed. Mater. Res., Part A*, 2017, **105**, 1618–1623.
10 K. Jin, L. Wang, K. Zhang, H. Ramaraju, S. J. Hollister and Y. Fan, *Biomacromolecules*, 2023, **24**, 2501–2511.
11 R. Akman, H. Ramaraju, M. Hollister, A. Verga and S. J. Hollister, *Polym. Sci. Technol.*, 2025, **1**, 132–143.
12 R. Qu, D. Zhou, T. Guo, W. He, C. Cui, Y. Zhou, Y. Zhang, Z. Tang, X. Zhang and Q. Wang, *Mater. Des.*, 2023, **225**, 111556.
13 M. Levin, Y. Tang, C. D. Eisenbach, M. T. Valentine and N. Cohen, *Macromolecules*, 2024, **57**, 7074–7086.
14 T. Y. Koh and A. Sutradhar, *Addit. Manuf.*, 2022, **56**, 102866.
15 Y. Zhang, C. Li, W. Zhang, J. Deng, Y. Nie, X. Du, L. Qin and Y. Lai, *Bioact. Mater.*, 2022, **16**, 218–231.
16 M. Bao, Q. Zhou, W. Dong, X. Lou and Y. Zhang, *Biomacromolecules*, 2013, **14**, 1971–1979.
17 A. Vashisth, S. T. Upama, M. Anas, J. H. Oh, N. Patil and M. J. Green, *Nanoscale Adv.*, 2021, **3**, 5255–5264.
18 K. Jin, H. Li, M. Liang, Y. Li, L. Wang and Y. Fan, *Regener. Biomater.*, 2023, **10**, rbad050.
19 S. Wu, M. Hua, Y. Alsaid, Y. Du, Y. Ma, Y. Zhao, C. Y. Lo, C. Wang, D. Wu and B. Yao, *Adv. Mater.*, 2021, **33**, 2007829.
20 X. Zhang, B. H. Tan and Z. Li, *Mater. Sci. Eng., C*, 2018, **92**, 1061–1074.
21 C. B. Sweeney, A. G. Moran, J. T. Gruener, A. M. Strasser, M. J. Pospisil, M. A. Saed and M. J. Green, *ACS Appl. Mater. Interfaces*, 2018, **10**, 27252–27259.
22 D. Debnath, X. Zhao, M. Anas, D. L. Kulhanek, J. H. Oh and M. J. Green, *Carbon*, 2020, **169**, 475–481.
23 A. Vashisth, R. E. Healey, M. J. Pospisil, J. H. Oh and M. J. Green, *Compos. Sci. Technol.*, 2020, **195**, 108211.
24 W. Bauhofer and J. Z. Kovacs, *Compos. Sci. Technol.*, 2009, **69**, 1486–1498.
25 Y. Zhang, S. Le, H. Li, B. Ji, M.-H. Wang, J. Tao, J.-Q. Liang, X.-Y. Zhang and X.-Y. Kang, *Biosens. Bioelectron.*, 2021, **194**, 113592.
26 E. W. Keefer, B. R. Botterman, M. I. Romero, A. F. Rossi and G. W. Gross, *Nat. Nanotechnol.*, 2008, **3**, 434–439.

27 M. Anas, M. M. Mustafa, A. Vashisth, E. Barnes, M. A. Saed, L. C. Moores and M. J. Green, *Appl. Mater. Today*, 2021, **23**, 101044.
28 J. T. Gruener, A. Vashisth, M. J. Pospisil, A. C. Camacho, J.-H. Oh, D. Sophiea, S. E. Mastroianni, T. J. Auvil and M. J. Green, *J. Manuf. Process.*, 2020, **58**, 436–442.
29 Y. Zhu, K. Deng, J. Zhou, C. Lai, Z. Ma, H. Zhang, J. Pan, L. Shen, M. D. Bucknor and E. Ozhinsky, *Nat. Commun.*, 2024, **15**, 1123.
30 G. C. Van Rhoon, T. Samaras, P. S. Yarmolenko, M. W. Dewhirst, E. Neufeld and N. Kuster, *Eur. Radiol.*, 2013, **23**, 2215–2227.